TECHNICAL ARTICLE

# Impact and Compression-After-Impact Performance of a Thin Z-Pinned Composite Laminate

L. Francesconi, G. Loi, and F. Aymerich ⓘ

Impact and compression-after-impact (CAI) tests were carried out on $[0_2/\pm45]s$ carbon/epoxy samples to characterize the effect of z-pinning on the delamination resistance and damage tolerance properties of the laminate. Unpinned and z-pinned samples were subjected to impacts between 2 and 36 J to produce damage conditions that extend from barely visible impact damage (BVID) to complete penetration. The damage induced by impact and the damage modes leading to ultimate CAI failure were examined by X-radiography and by direct observations of the sample faces during CAI loading. The analyses indicate that the role of z-pins on the impact and CAI response of the laminate is dependent on the size and features of the damage. Z-pins do not modify the structural response to impact of the laminate, but they are effective in reducing the extent of damage for impact energies above a threshold value. Z-pinning is also effective in improving the CAI strength of the laminate for impact energies above this threshold value, even though it degrades the residual compressive strength for lower impact energies. Reductions in impact delamination size of up to 50% and improvements in CAI strength of about 20% were achieved by z-pinning for high-energy impacts. The mechanisms by which the z-pins affect the CAI response of the samples are illustrated and examined in detail for different impact damage severities.

## 1. Introduction

In spite of the many advantages offered by polymer composite laminates over more traditional metallic materials (i.e., high specific stiffness and strength, remarkable fatigue properties, good corrosion resistance, superior design flexibility), their sensitivity to impact loads is a serious obstacle to a wider adoption in critical load-carrying components.

In contrast to metals, which may absorb a significant amount of impact energy by irreversible plastic deformation, the key mechanisms for energy dissipation in composite materials consist of fracture modes, such as matrix cracking, delaminations and fiber fracture, which may significantly affect the strength performance of the material (Ref 1). Delaminations, in particular, have a major influence on the compressive response of laminated composites,

which can be drastically degraded by the occurrence of local buckling of the delaminated layers prior to final collapse (Ref 2).

An effective method to improve the resistance to delamination of composites involves the insertion of reinforcement through the thickness (z-direction) of the laminate, either by the adoption of 3D fiber preforms (3D weaving, braiding, knitting) or by the introduction of selective translaminar reinforcement in a conventional 2D laminate (z-pinning, stitching). The z-pinning technique consists in inserting small pins or rods, usually made of carbon composite or steel, orthogonally to the uncured prepreg stack before consolidation (Ref 3-5). Z-pins improve the resistance to delamination by applying bridging tractions between delaminated layers, thus reducing the driving force available for crack growth (Ref 6-10). Extensive experimental evidence shows that the increased delamination toughness translates into improvements in various mechanical properties such as impact damage resistance, damage tolerance, joint strength, load-bearing capacity (Ref 11-18). On the other hand, tensile, compressive, and bending strengths of laminates are generally reduced by z-pinning under static or cyclic loads (Ref 12, 16, 19-21). These reductions are mainly attributed to the microstructural degradation modes generated by the insertion of z-pins, such as resin rich regions and clusters of broken fibers (which may act as crack initiation sites), as well as fiber waviness and crimping (which promote microbuckling and kinking of compression-loaded fibers).

A fair amount of research has been conducted to explore the influence of z-pins on the low-velocity impact behavior of composite laminates (Ref 7, 12, 16, 17), even though only a few studies (Ref 14, 22-24) have examined their role across a range of impact energies wide enough to result into damage conditions markedly different in size and main failure modes. The results of these studies consistently indicate that z-pins do not prevent the initiation of delamination and only become able to restrain delamination growth when a large-scale z-pin bridging zone forms

---

**L. Francesconi**, Logitech Europe-EPFL, Lausanne, Switzerland; and **G. Loi** and **F. Aymerich**, Department of Mechanical, Chemical and Materials Engineering, University of Cagliari, Cagliari, Italy. Contact e-mail: francesco.aymerich@dimcm.unica.it.

in the wake of the delamination front, with ensuing reductions in damage size generally increasing with increasing impact energy. Extremely limited research work has been carried out on the compression-after-impact (CAI) behavior of z-pinned laminated composites, with almost all investigations (Ref 4, 22, 23) exploring the CAI response of thick laminates (4 mm and thicker). Quasi-isotropic carbon/epoxy laminates with a thickness of 4 mm were for example examined in (Ref 4) to assess the enhancement in CAI properties achievable by z-pinning. The samples were z-pinned with areal densities of 2 and 4% in a central region of 25 × 25 mm and subjected to impacts with three energies (10, 15 and 20 J). Improvements in the CAI strength of about 55% and 110% were obtained after impacts of 15 J for samples, respectively, reinforced with 2% and 4% pin density. The CAI response of 4-mm- and 6-mm-thick quasi-isotropic carbon/epoxy laminates z-pinned with an areal density of 2% was investigated in (Ref 22). The introduction of z-pins significantly improved the post-impact performance of the laminates, with increases in residual compressive strength of about 45% in samples impacted at energies between 15 and 40 J. The results of the tests conducted in (Ref 23) on 4.3-mm-thick quasi-isotropic carbon/epoxy laminates show that z-pinning improved the residual compression strength after high-energy impacts (an average increase in CAI strength of about 8% was achieved in samples with a 2% z-pin content for 25.5 J impacts), while it was ineffective after low-energy (8.5 J) impacts.

Beside the little information available in the literature on the CAI behavior of thick z-pinned laminates, there is an almost complete lack of experimental data and observations on the role of z-pins on the post-impact performances of thin laminates, which typically exhibit impact and CAI responses different from those of thick laminates.

To address this lack of knowledge, the authors have recently started an experimental program to characterize the effect of z-pinning on the CAI properties of thin composite laminates. A first series of experimental tests performed on 2.5-mm-thick quasi-isotropic and cross-ply laminates with increasing impact damage severities (Ref 18) showed that, for both layups, the compressive strength was degraded by z-pinning below a threshold impact energy, whereas it was significantly improved above this threshold value. The study also revealed that a strict dependence exists between the extent and the features of the impact damage mechanisms and the role of z-pins on the damage progression leading to CAI failure.

As an extension of this previous study and with the aim of improving our understanding of the damage mechanics of thin z-pinned composites, this paper examines the effect of z-pinning on the impact and post-impact compressive response of a thin $[0_2/ \pm 45]$s carbon/epoxy laminate, which is characterized by impact damage scenarios that differ in size, shape and number of delaminated interfaces from those previously investigated in (Ref 18). The correlation between the failure modes introduced by the impact and the sequence of the damage mechanisms leading to CAI failure is examined for impact damage conditions ranging from barely visible impact damage (BVID) to complete penetration of the indentor into the laminate thickness.

## 2. Experimental

The material investigated in this study was a $[0_2/ \pm 45]$s carbon–epoxy laminate made of unidirectional prepreg layers with 62% fiber weight content (Texipreg® HS300/ET223). The laminates were consolidated in autoclave under vacuum with a cycle consisting of a 35 min heating ramp up to a temperature of 125 °C, a 60 min dwell time, and a final 30 min cooling ramp to room temperature. Rectangular samples 65 mm × 88 mm in size and 2.5 mm thick were cut from the cured panels for impact and CAI testing.

Before consolidation, some of the laminates were z-pinned using carbon/BMI Z-FIBER© pins of 0.51 mm diameter, supplied by Albany Engineered Composites (Rochester, NH, USA) with a square grid pattern (3.1 mm spacing for an areal density of 2%) within a polymer foam carrier. The z-pins were inserted into the laminate with the aid of an ultrasonic gun (Branson LPX20), operated at a frequency of 20 kHz and an energy of 1 kJ/cycle. After the insertion process, the protruding lengths of the z-pins were trimmed off using a sharp blade. The laminates were selectively pinned on 20 mm by 60 mm rectangular regions so as to obtain, after cutting, samples with a z-pin reinforced area centered on the impact location (Fig. 1).

The impact tests were carried out on a drop-weight testing machine developed in-house (Fig. 2), which consists of a drop tower with two vertical rod guides, an impactor running on the guides through linear roller bearings, and an anvil with a sample support fixture. The system is provided with an automatic mechanism that captures the impactor to prevent repeated impacts in case of a rebound. The impactor used for the tests had a mass of 2.28 kg and was provided with a hemispherical indentor of 12.5 mm in diameter. During impact, the specimens were supported on a steel frame with a 45 × 68 mm rectangular opening and were restrained to the support by four soft rubber clamps. The velocity of the impactor at the instant of contact with the sample was measured by an infra-red sensor, while the contact force was measured by a full bridge of semiconductor strain-gauges bonded to the indentor. The force signal was acquired at a sampling rate of 150 kSa/s, and the displacement of the indentor was evaluated by integration of the contact force history.

The samples were impacted with energies varying between 2 and 35 J (corresponding to impact velocities between about 1.3 and 5.5 m/s) to examine the changes introduced by z-pins on the impact and CAI behavior of the samples for increasing damage severities. In particular, the selected range of impact energies allowed to cover the entire domain of the typical damage scenarios that can be realistically expected under low-velocity impact loadings (i.e., onset of interlaminar and intralaminar matrix cracks at single layers and interfaces, growth of major delaminations at multiple interfaces, initiation of perforation by major fiber fracture, through-thickness penetration). A summary of the samples tested during the study is reported in Table 1.

The compression-after-impact (CAI) tests were carried out using the anti-buckling fixture illustrated in Fig. 3 and following the general guidelines provided by the ASTM Standard D7137-12 (Ref 25). Because of the small thickness of the examined laminates (2.5 mm as compared to the 4 to 6 mm range covered by the ASTM standard), samples with a scaled-down size (65 mm × 88 mm vs the 100 mm × 150 mm size indicated by the ASTM standard) were chosen to avoid the use of frontal anti-buckling supports that may interfere with the progression of damage from the impact region. The samples, supported by knife edges along the longer sides, were end-loaded until failure with a 250 kN Instron servo-electric machine operated at a stroke speed of 1 mm/min. Small fiberglass tabs were bonded onto the ends of the samples to
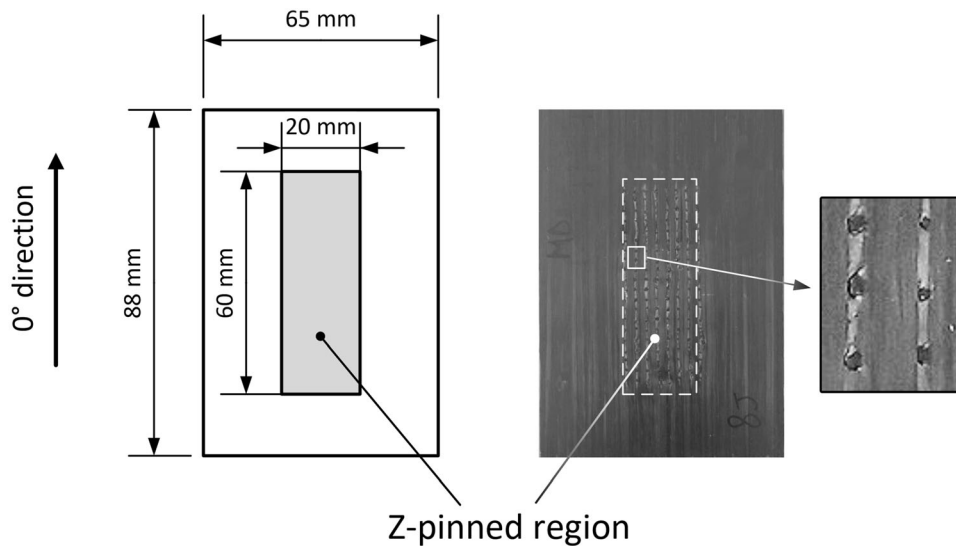
**Fig. 1** Samples and size of z-pinned region
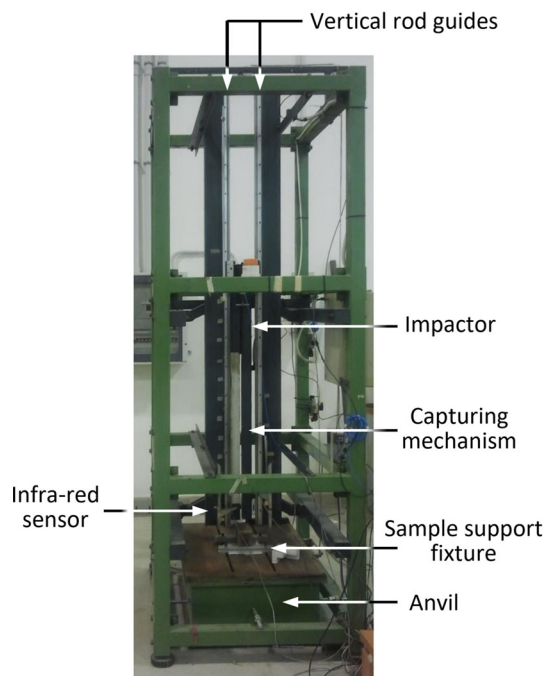


**Fig. 2** Drop-weight testing machine used for low-velocity impact tests

avoid or restrain crushing damage in the loading zone, which could develop, especially with limited impact damage, because of the small thickness of the laminates.

The damage generated by the impact and by the CAI loading was assessed by penetrant enhanced x-ray radiography and visual observation of the sample surfaces. To this end, the samples were immersed in a radio-opaque zinc iodide solution for 6 h and then x-rayed using a Faxitron 43855A cabinet x-ray system. The radiographic images were obtained on AGFA NDT D4 films placed directly below the composite. The voltage of the x-ray source, the irradiation time and the tube current were, respectively, 20 kVp, 100 s and 3 mA, for a distance between the x-ray source and the sample of 60 cm.

The depth of the permanent indentation resulting from the impact, which is a parameter frequently used in damage tolerance procedures in the aeronautical field, was also measured using a digital dial gauge with a resolution of 0.01 mm. The dial gauge was moved across the impacted surface of the sample, and the indentation depth was evaluated as the maximum difference between the readings at the indented region and the average of the readings at the surface of the sample far from the impact region.

## 3. Results and Discussion

### 3.1 Low-Velocity Impact Tests

Force–deflection curves acquired on unpinned and z-pinned samples impacted at different energies are presented in Fig. 4. An example of the good repeatability of the impact response of the laminates is visible in the graphs of Fig. 5, which compare the force–deflection curves of different unpinned and z-pinned samples impacted with an energy of 8 J.

The plots of Fig. 4 show that the laminates exhibit smooth loading and unloading responses for very low impact energies (Fig. 4a), while for impact energies of about 8 J high-frequency force oscillations may be seen from a level of about 4 kN (Fig. 4b). When the impact energy exceeds a threshold of approximately 15 J, the impact force shows a large and sudden drop followed by large amplitude fluctuations (Fig. 4c). This abrupt load drop corresponds to the initiation of the perforation process, with major fiber fracture occurring at the contact region below the indentor. If the energy of the impact is further increased to values close than 30 J (Fig. 4d), the force–displacement traces show an unloading stage characterized by increasing displacements, which signals the penetration of the indentor through the entire laminate thickness without any rebounding.

The perforation process is thus triggered by the initiation of significant fiber failure at the contact region and proceeds by progressively fracturing the fibers of the adjacent layers until the penetration begins when all layers are pierced by the

**Table 1    Summary of tested samples**

| Impact energy, J | Drop height, m | Impact velocity, m/s | Number of unpinned samples | Number of z-pinned samples |
|---|---|---|---|---|
| 2 | 0.089 | 1.33 | 2 | 2 |
| 4 | 0.179 | 1.87 | 2 | 2 |
| 6 | 0.269 | 2.29 | 2 | 3 |
| 8 | 0.358 | 2.65 | 3 | 3 |
| 12 | 0.537 | 3.24 | 2 | 2 |
| 16.5 | 0.738 | 3.80 | 3 | 3 |
| 24 | 1.074 | 4.59 | 3 | 4 |
| 30 | 1.343 | 5.13 | 3 | 3 |
| 35 | 1.567 | 5.54 | 3 | 3 |

Impact energy, drop height and impact velocity columns report nominal values; slight differences may occur between the nominal values and the actual values measured on the single tests.
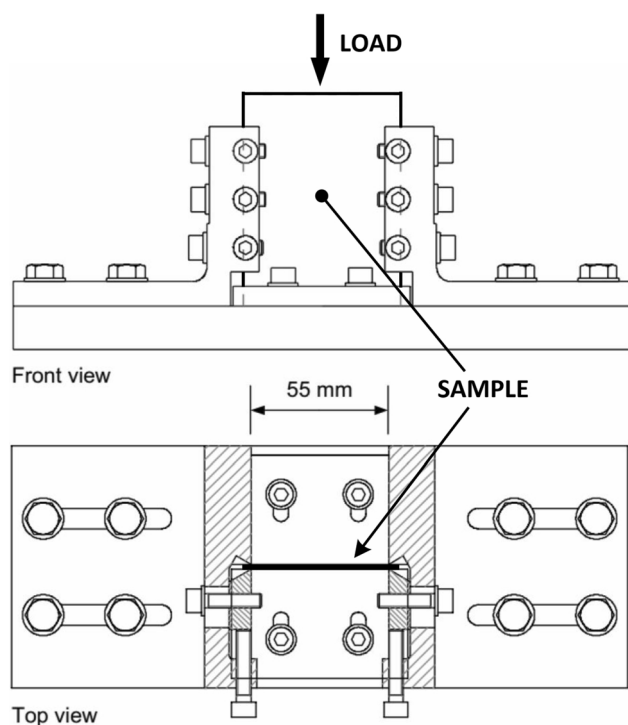


**Fig. 3**    Anti-buckling fixture used for CAI tests

indentor. The onsets of the perforation and penetration stages are easily identified in the force–deflection curves as the instants at which, respectively, the force exhibits a sudden load drop (Fig. 4c) or levels off to an approximately constant value with increasing deflection (Fig. 4d). Average threshold energies of about 15 J and 29 J, calculated as the energies lost by the impactor up to these two instants, were obtained, respectively, for the perforation and penetration conditions.

The trends of the values of the peak force and of the energy dissipated during the impact are plotted as a function of impact energy in the graphs of Fig. 6. We see (Fig. 6a) that the peak force (which is representative of the load-bearing capacity of the laminate) keeps increasing with impact energy until it reaches a plateau at the threshold perforation energy. On the other hand, the absorbed energy (Fig. 6b) shows a continuously rising trend over the entire impact energy span. The absorbed energy, evaluated as the energy lost by the impactor, may be considered a measure of the energy dissipated through the different internal damage mechanisms and also spent by friction during the penetration phase for high-energy impacts.

The graph of Fig. 7 presents the values of the residual indentation depth measured after impact in samples that were not penetrated by the indentor (i.e., for energies below the threshold penetration energy of about 29 J). As expected, the indentations exhibit a sudden increase as soon as the impact energy exceeds the critical value for the onset of perforation.

The experimental data presented in the graphs of Fig. 6 and 7 clearly demonstrate that z-pinning is not capable of providing appreciable enhancements of the impact behavior of the laminate, neither with regard to its structural response nor with regard to its resistance to perforation and penetration.

On the other hand, the X-radiographs of Fig. 8, which show the internal damage patterns of unpinned and z-pinned laminates impacted at different energy levels, indicate that the presence of z-pins has a beneficial influence on the delamination resistance of the laminate, with the exception of very low impact energies.

The x-ray images show that, in both unpinned and pinned laminates, the initial damage for an impact energy of 2 J consists of matrix cracking in the 0° plies farthest from the impact side and in the ± 45° layers, together with small delaminations on the two interfaces (− 45°/ + 45° and + 45°/ 0°) adjacent to the lower + 45° layer. With increasing impact energy, these delaminations (notably the one between the + 45° and 0° layers) grow in size and additional delaminations develop at the remaining 0°/ + 45° and + 45°/− 45 interfaces. Some limited fiber fracture, which gives rise to the high-frequency oscillations visible in the force signal, is first observed for energies of about 8 J at the contact area of the impacted 0° layer. It is also seen that in z-pinned laminates the paths of broken fibers always start at pin sites at the contact region. Impacts with energies of 16.5 J give rise to extensive fiber breakage on the impacted layers and induce significant delaminations at all four interfaces. As mentioned before, the extensive fiber failures are responsible for the large force drop observed in the force–displacement traces (see Fig. 4c). Impacts with energy of about 29 J and above finally lead to penetration of the indentor into the sample, with responses characterized by "open" force–displacement traces, as opposed to the typical "closed" curves of lower energy impacts (Fig. 4d). Further details on the damage mechanisms induced by impact may be found in (Ref 14).
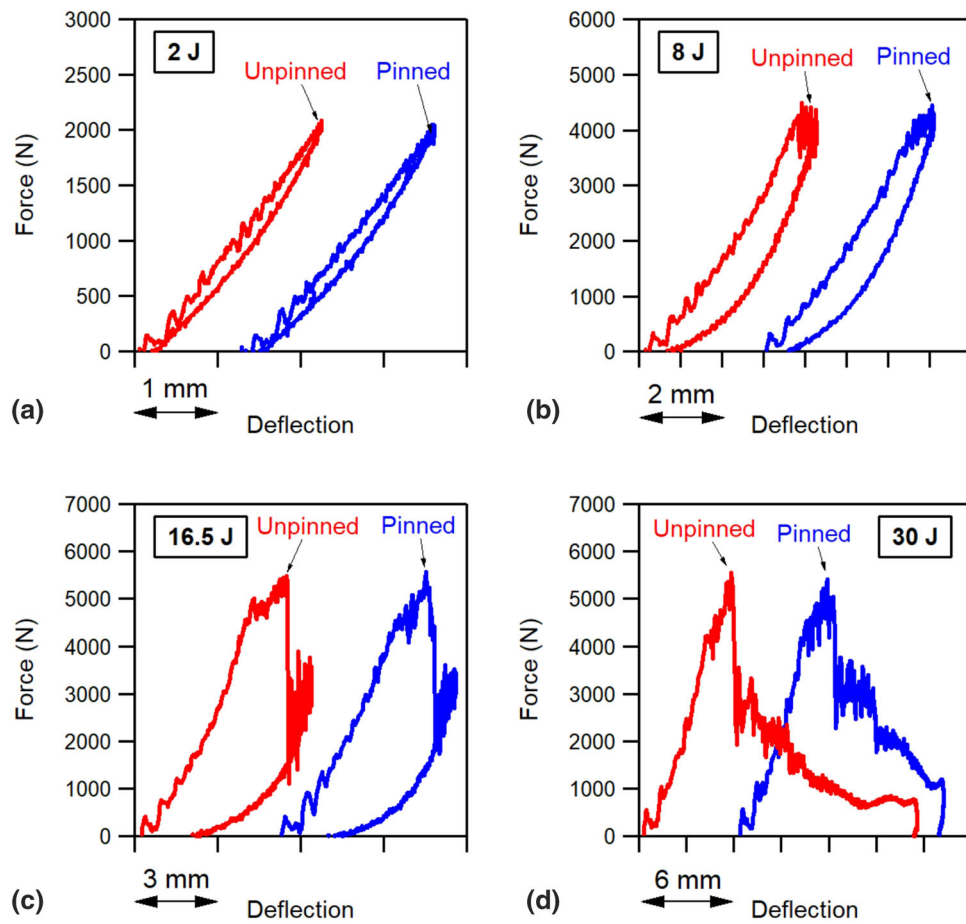
**Fig. 4** Force–deflection curves recorded on unpinned and z-pinned samples during impacts with different energies. The pinned curves are shifted for clarity
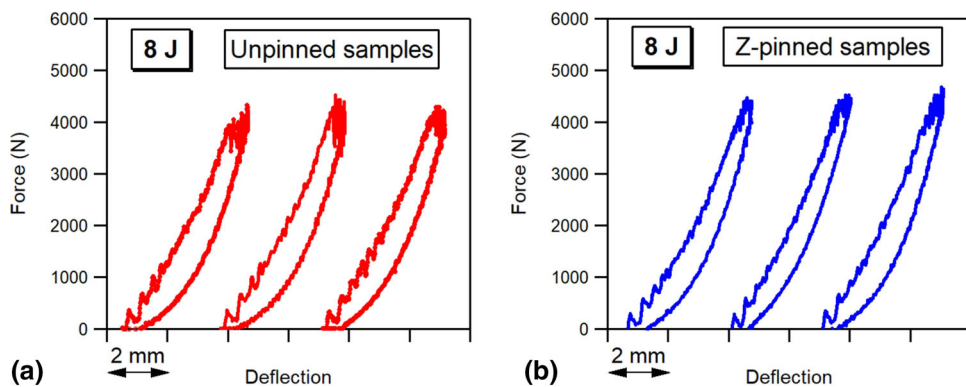


**Fig. 5** Force–deflection curves recorded on unpinned (a) and z-pinned (b) samples during 8 J impacts. The curves are shifted for clarity

A simple comparison of the radiographic images of unpinned and z-pinned samples reveals that, except for impacts with very low energy, the delaminated area of z-pinned samples is smaller than that of unpinned samples and that the reduction in delamination size achieved by z-pinning increases with increasing impact energies. For a more comprehensive comparison, the projected delamination areas measured on X-radiographs of unpinned and z-pinned specimens are plotted as a function of impact energy on the graph of Fig. 9. The trends of the damaged areas reported in the graph show that the toughening mechanism of z-pins becomes effective only for

impact energies above a certain level. While unpinned and z-pinned laminates have comparable damage areas for impacts with energies below about 6 J, for energies above this value the rate of damage growth with impact energy is greatly reduced by z-pinning. In particular, the damage areas of z-pinned laminates exhibit an almost flat trend for impact energies higher than 12 J, as opposed to the much steeper rise of unpinned laminates. This typical behavior, observed in various investigations on the impact damage response of composite laminates with various kinds of through-thickness reinforcement (Ref 14, 22-24, 26, 27), is a direct consequence of the fact that a sufficiently large
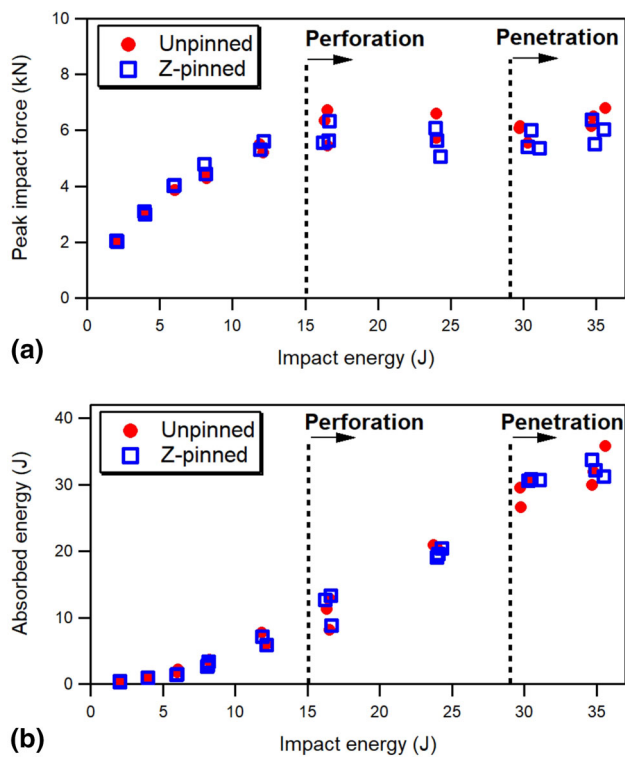
**Fig. 6** Peak impact force (a) and absorbed energy (b) vs impact energy in unpinned and z-pinned laminates
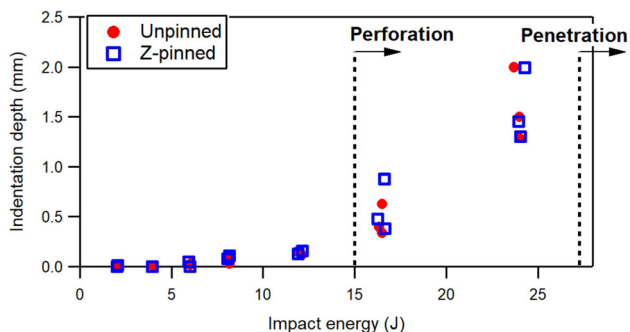


**Fig. 7** Indentation depth vs impact energy in unpinned and z-pinned laminates

delamination crack is required before the z-pins may effectively apply traction loads between the delaminated layers.

It may be also worth noting that the reduction in delamination size achieved by z-pinning for impacts above a certain energy does not translate into lower absorbed energies, as seen by comparing the data reported in the graphs of Fig. 6 and 9. This indicates that in z-pinned laminates a significant fraction of the energy dissipated during the impact is spent in damage mechanisms directly associated with the presence of z-pins, such as matrix cracking or growth of broken fibers at pin sites, as well as debonding, pullout and failure of z-pins.

### 3.2 Compression-After-Impact (CAI) Tests

The graphs of Fig. 10 show stress–displacement traces recorded during CAI tests on unpinned and z-pinned laminates impacted at the four energies examined in the previous section (see Fig. 4 and 8). The stress was calculated as the applied

force divided by the cross-sectional area of the sample. The chosen impact energies can be associated with the four characteristic damage conditions of increasing severity that were observed over the explored energy span. In particular, only minor matrix cracking and small delaminations are caused to samples by 2 J impacts (Fig. 8a), while much more extensive delaminations and early fiber fractures develop in samples impacted at 8 J (Fig. 8b). Perforation damage, where the fibers of many top layers are broken by the indentor leading to a large indentation depth, occurs for 16.5 J impacts (Fig. 8c). Complete penetration of the laminate characterizes the damage induced by the 30 J impacts (Fig. 8d).

The CAI strengths of all tested samples are plotted against impact energy in the graph of Fig. 11. The graphs of Fig. 10 and 11 show that the CAI performance of z-pinned samples is worse than that of unpinned samples for impact energies below a threshold of about 6 J, but z-pins start improving the CAI strength of the laminates for higher impact energies. An increase in CAI strength of approximately 20% is recorded after z-pinning for impact energies in the perforation-penetration damage regime. Similar trends were observed in a previous study for the CAI response of cross-ply ($[0_2/90_2]s$) and quasi-isotropic ($[0/ \pm 45/90]s$) laminates made of the same prepreg material (Ref 18).

The sequence of the failure and deformation events that led to CAI collapse of the laminates was reconstructed by examining the images of the faces of the sample acquired by a digital camera during the compression loading and by comparing the X-radiographs of damage taken before and after the CAI test. The results of these observations will be illustrated in the following with reference to three impact energies (4 J, 8 J and 24 J) chosen to assess the role of Z-pinning in the presence of three markedly distinct impact damage conditions, respectively, characterized by small delamination damage, extensive delamination with minor fiber fracture, perforation damage, as illustrated in the previous section.

The progressions of the damage mechanisms observed under compression on the front (impact) and rear face of unpinned and z-pinned laminates subjected to 4 J impacts are shown in Fig. 12 and 13. We see that, because of the small size of the delaminated areas, no significant buckling of the delaminated layers occurs on the rear face of both unpinned and pinned samples before final failure (it may be worth noting that possible out-of-plane instabilities are expected to first occur at the rear face of the laminate, since the largest impact delaminations affect the interfaces closer to that side). The strength of the samples appears to be essentially controlled by the fracture of 0° fibers at the indentation area. In unpinned samples the first occurrence of fiber fracture immediately triggers the catastrophic failure of the laminate by the immediate propagation of broken fibers in the transverse direction (Fig. 12). Conversely, in z-pinned samples the manufacturing defects introduced during the z-pinning process (notably the clusters of broken fibers) promote the earlier development at z-pin sites of new fiber failures (Fig. 13), which exhibit a short but noticeable stage of progressive growth until their unstable propagation leads to the final collapse. Therefore, when the extent of impact damage is small, the post-impact compressive strength of z-pinned laminates is lower than that of unpinned laminates, as a direct consequence of the adverse effect of the microstructural distortions and localized fiber damage generated by the insertion of z-pins. X-radiographs of damage taken before and after the CAI test in unpinned and z-pinned laminates are compared in Fig. 14 and 15. It must be noted that
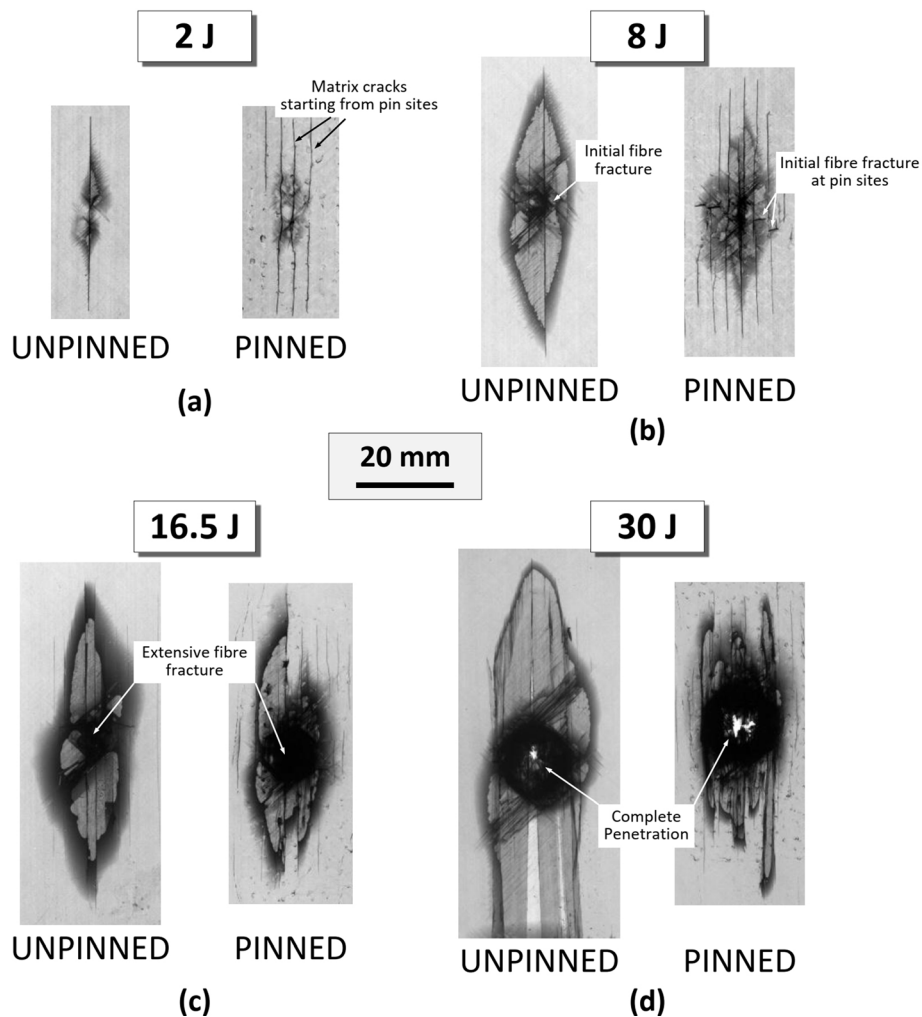
**Fig. 8** X-radiographs of unpinned and z-pinned samples impacted ad different energies
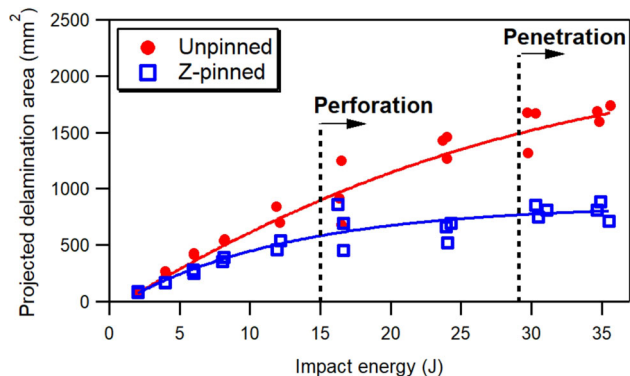


**Fig. 9** Projected delamination area vs impact energy in unpinned and z-pinned samples

the large delaminated areas visible across the paths of fractured fibers both in the unpinned sample and outside the z-reinforced region of the pinned sample only develop as a secondary effect of the unstable fiber failure growth leading to the final collapse, as suggested by the examination of the sample faces acquired during the CAI loading. We may also see that the propagation of the delamination is almost completely inhibited in the central z-reinforced region of the pinned sample (Fig. 15), thus showing

the high effectiveness of Z-pins for improving the delamination resistance.

Sequences of deformation and failure events recorded at different stages of the compressive load and x-ray images acquired before and after ultimate CAI failure are shown in Fig. 16, 17, 20, 21, 22 and 23 for unpinned and z-pinned samples impacted at 8 J and 24 J.

In unpinned samples impacted at 8 J (Fig. 16 and 17), the compressive load induces the progressive out-of-plane deflection of the 0° delaminated layers at the rear face of the laminate. This localized buckling is expected to result in a continuous increase in the fraction of load carried by the 0° layers at the impact side of the laminate; the ultimate failure finally occurs when the pre-existing fiber failures caused by the indentor during the impact event grow unstably to the edges of the laminate.

In z-pinned samples (Fig. 18), because of the much smaller delaminated area (see Fig. 9) and of the presence of through-thickness reinforcements, the buckling of the delaminated region is greatly restrained in comparison to unpinned samples. The load transfer subsequent to this very localized instability is therefore much less pronounced than in unpinned laminates and this results in a significantly better CAI performance, although the mechanism that triggers the ultimate failure (i.e., unstable propagation of pre-existing fiber fracture at the indentation area) is the same as for the unpinned laminates.
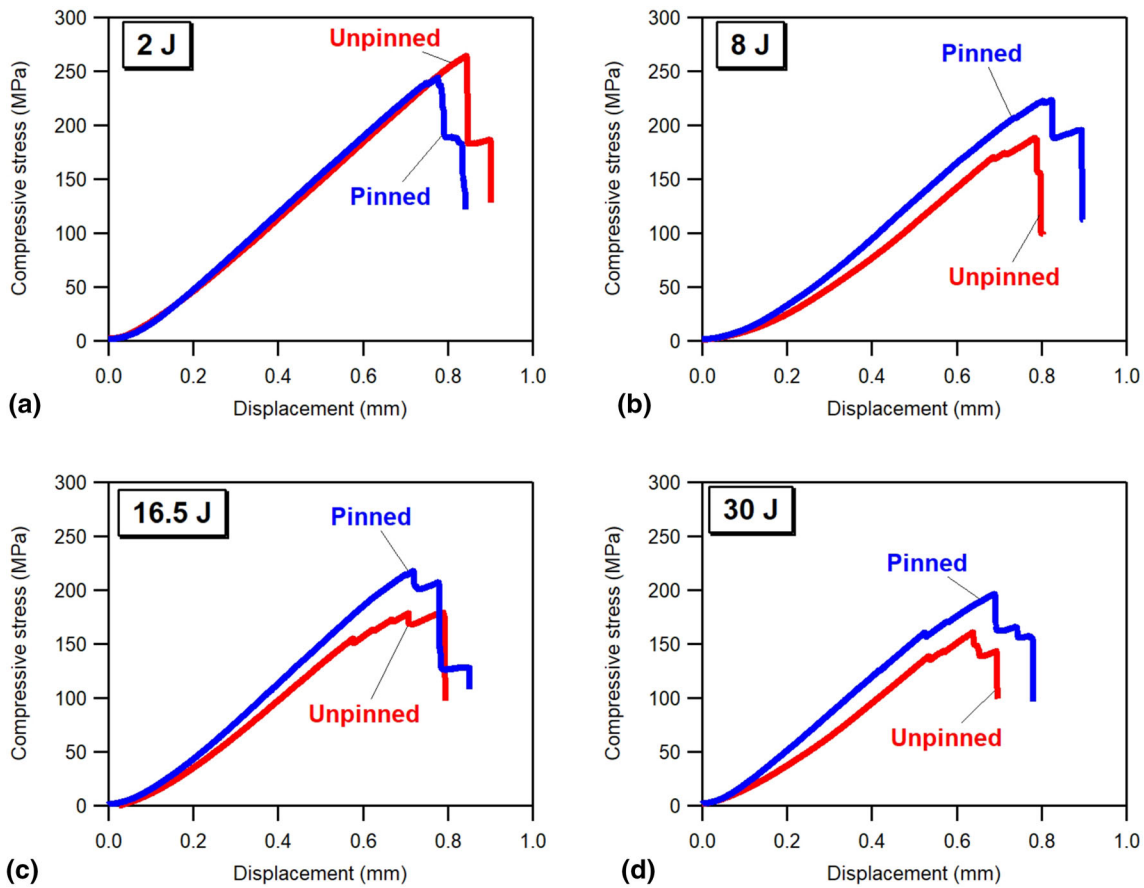
**Fig. 10** Force–displacement curves recorded during CAI loading on unpinned and z-pinned samples impacted at different energies
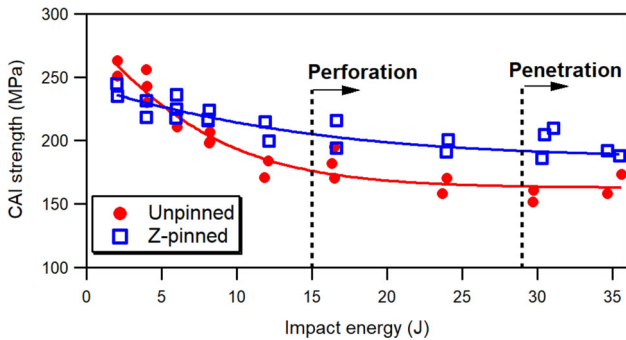


**Fig. 11** CAI strength vs impact energy for unpinned and z-pinned samples

The observations carried out during the entire CAI load history again indicate that the newly formed delaminated areas visible in the X-radiographs taken after the CAI tests (Fig. 17 and 19) only develop after the unstable growth of 0° broken fibers, while the comparison of the X-radiographs of unpinned and pinned samples confirms the excellent ability of z-pins to prevent the growth of delaminations under compressive loads.

Figure 20, 21, 22 and 23 illustrates the progressions of damage events recorded for samples impacted at an energy of 24 J, characterized by damage severities well within the perforation range, with major fiber fracture starting from the impact side and affecting several adjacent layers.

We note that the delaminated region at the + 45°/0° interface of the unpinned sample undergoes local instability (Fig. 20), with the formation of a large surface buckle on the rear face of the laminate. In this case, fiber fracture on the impact side exhibits a stable growth stage, with delaminations developing afterward in the adjacency of the broken fiber path (Fig. 21).

In pinned laminates (Fig. 22 and 23), because of the bridging effect of z-pins, the rear surface buckle is again much reduced in size in comparison with unpinned laminates. In addition to the beneficial effect of the reduced impact delamination size, z-pins also tie together adjacent layers at delaminated regions during the compressive load, thus resulting in an increase in bending stiffness and load-carrying capacity as compared to analogous unpinned laminates. The transfer of load from the 0° layers at the rear side of the sample to the load-carrying layers at the front side is expected to be less severe than in unpinned laminates, thus explaining the higher residual strength of z-reinforced laminates.

As a general remark, it is important to note that the improvement in CAI strength achieved by z-pinning for medium to high impact energies cannot be simply attributed to the smaller size of the impact-induced delaminated area. If we examine the CAI strengths as a function of delamination extent (Fig. 24), we may see, despite the large scatter typical of CAI tests, that the global trends of the unpinned and z-pinned data exhibit two clearly different slopes. For small delamination areas (i.e., for low impact energies), the CAI strengths of z-pinned laminates are lower than those of unpinned laminates, as
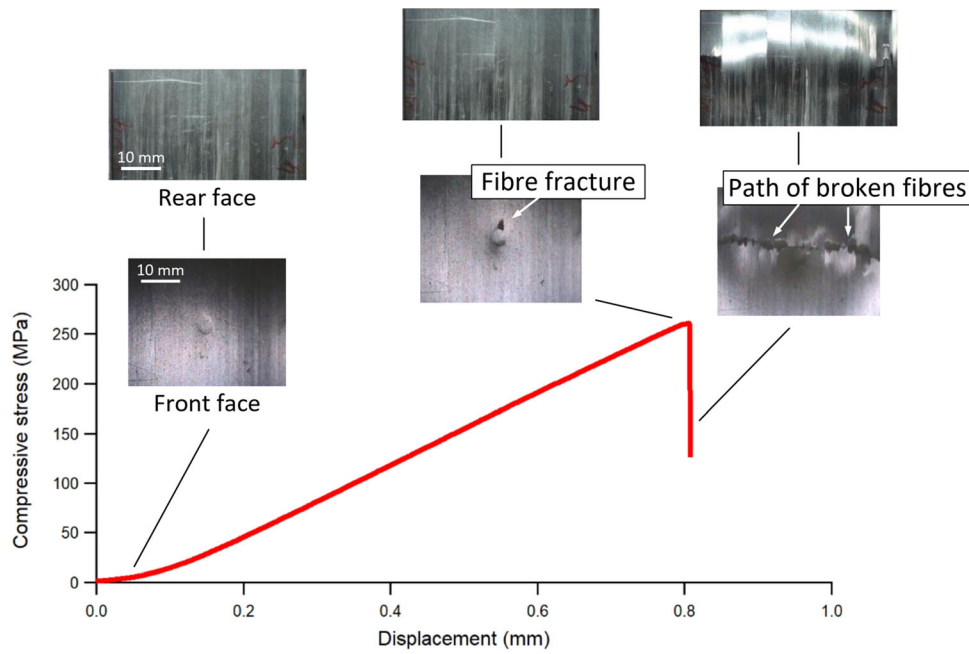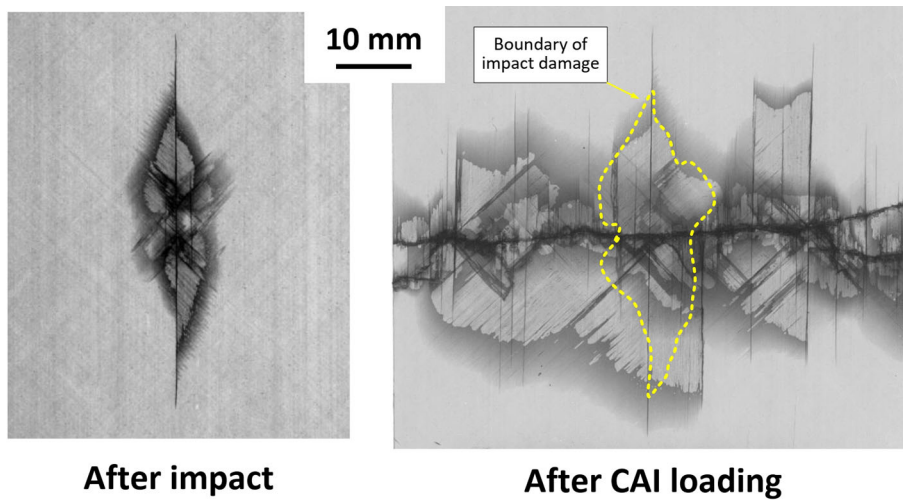
**Fig. 12** Progression of damage mechanisms observed during CAI loading on the front and rear faces of an unpinned sample impacted at 4 J
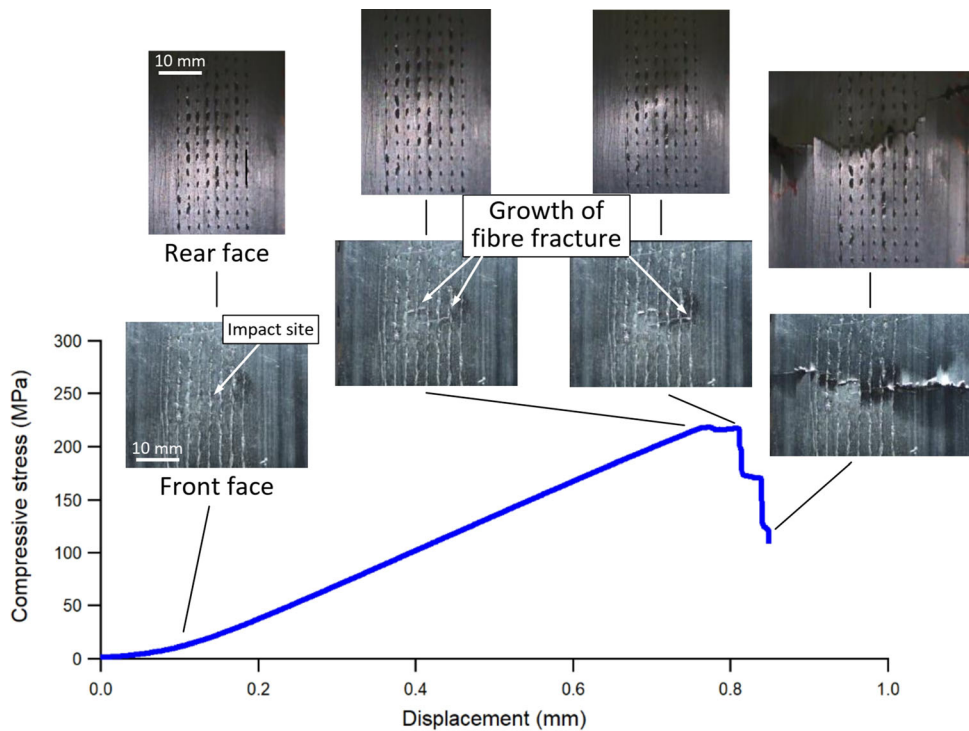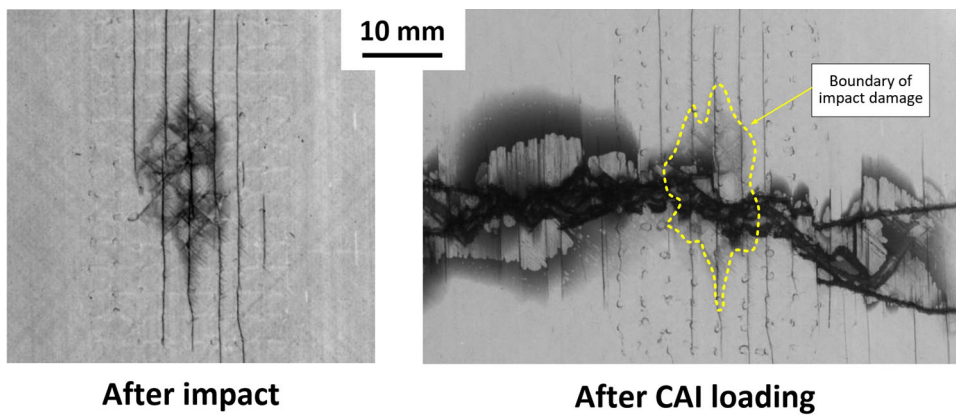


**Fig. 13** Progression of damage mechanisms observed during CAI loading on the front and rear faces of a z-pinned sample impacted at 4 J

a consequence of the detrimental effect of the localized damage introduced during the z-pinning process. Conversely, for large delamination areas (i.e., for high-energy impacts) the CAI strengths of z-pinned samples tend to be higher than those of unpinned samples with similar delamination extents. This shows that, in addition to the reduction in impact delamination size, further beneficial mechanisms, such as the stiffening and stabilizing action of z-pins on delaminated layers, play a significant role in enhancing the post-impact compressive response of the z-pinned laminate for high-energy impacts.

**Fig. 14** X-radiographs of an unpinned sample impacted at 4 J acquired before (left) and after CAI loading (right)
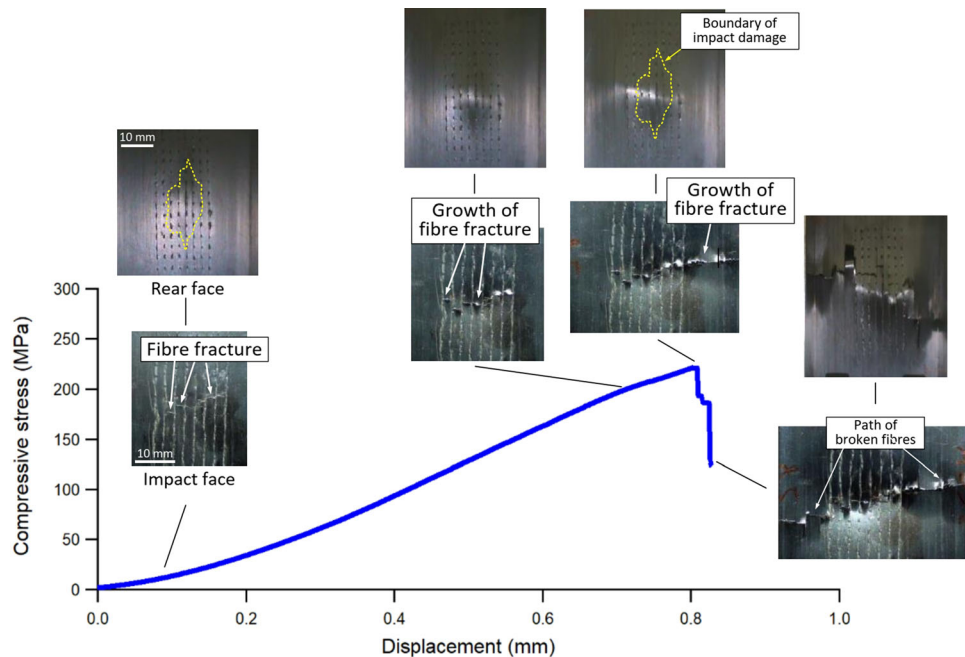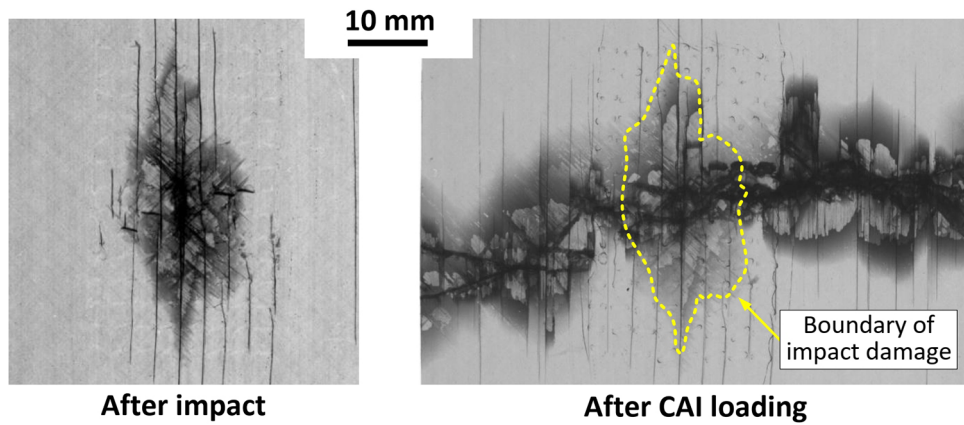


**Fig. 15** X-radiographs of a z-pinned sample impacted at 4 J acquired before (left) and after CAI loading (right)
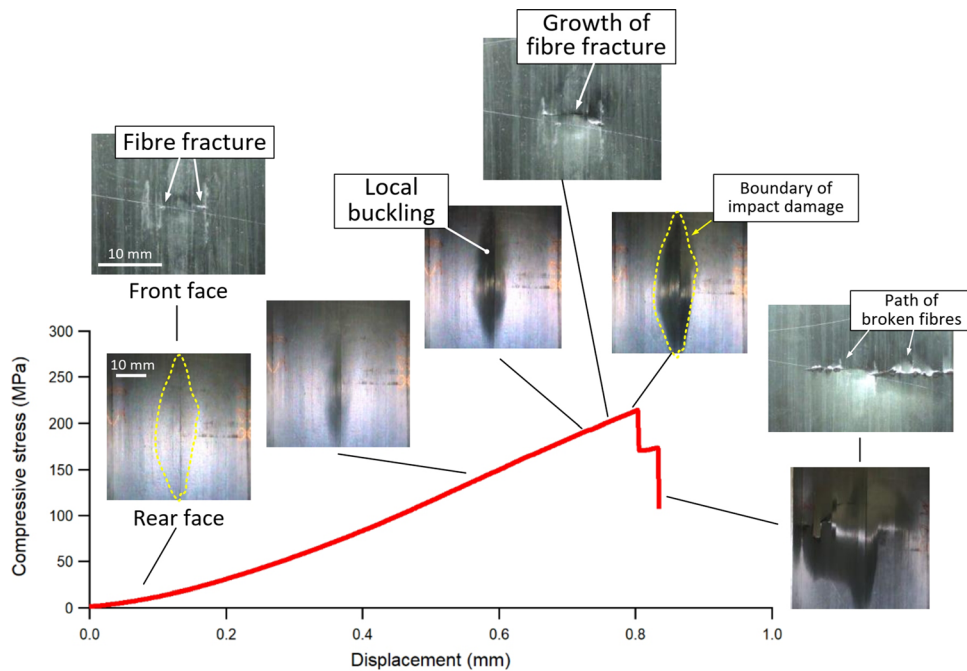


**Fig. 16** Progression of damage mechanisms observed during CAI loading on the front and rear faces of an unpinned sample impacted at 8 J
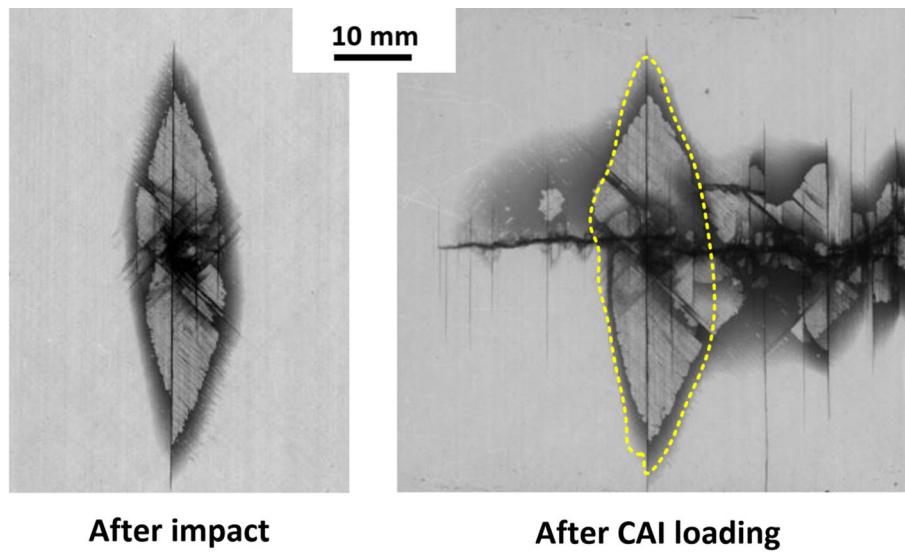
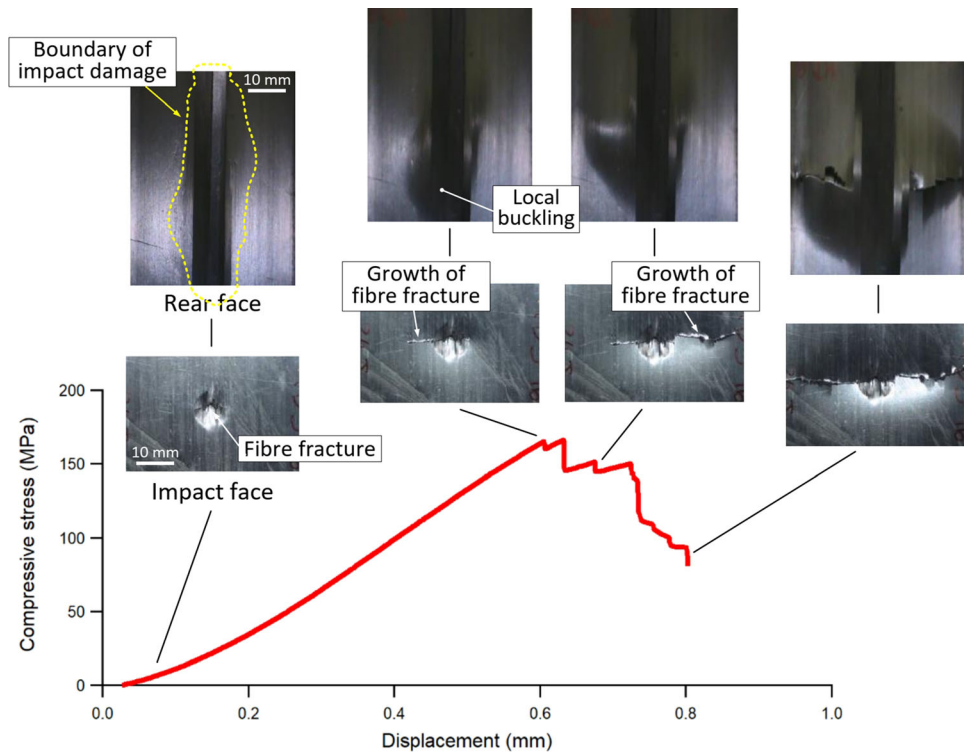**Fig. 17** X-radiographs of an unpinned sample impacted at 8 J acquired before (left) and after CAI loading (right)



**Fig. 18** Progression of damage mechanisms observed during CAI loading on the front and rear faces of a z-pinned sample impacted at 8 J

## 4. Conclusions

An experimental study has been carried out on the influence of z-pinning on the impact and CAI behavior of a thin $[0_2/\pm 45]_S$ carbon/epoxy laminate. The investigation was aimed at characterizing the mechanisms by which z-pins enhance the resistance to impact damage and affect the sequence of failure events that control the CAI strength for impact damage conditions ranging from BVID to full penetration.

The main indications provided by the experimental observations can be summarized as follows.

(1)  The efficacy of z-pinning for improving the impact damage resistance and the CAI strength of the laminate is greatly dependent on the impact energy imparted to the laminate.
(2)  Z-pins do not reduce the delamination size under impacts with energy below a threshold value of about 6 J;
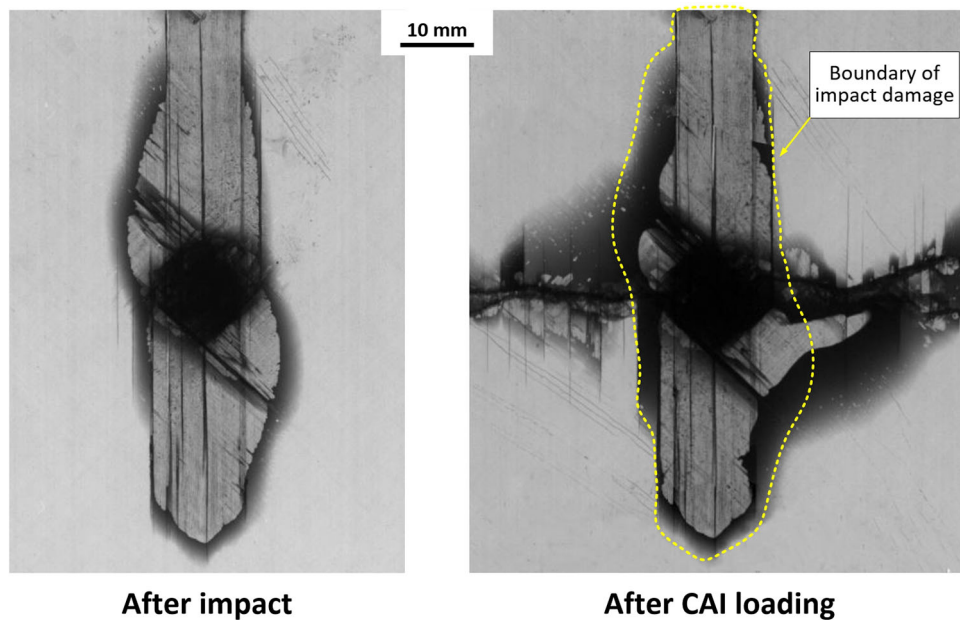
**Fig. 19** X-radiographs of a z-pinned sample impacted at 8 J acquired before (left) and after CAI loading (right)
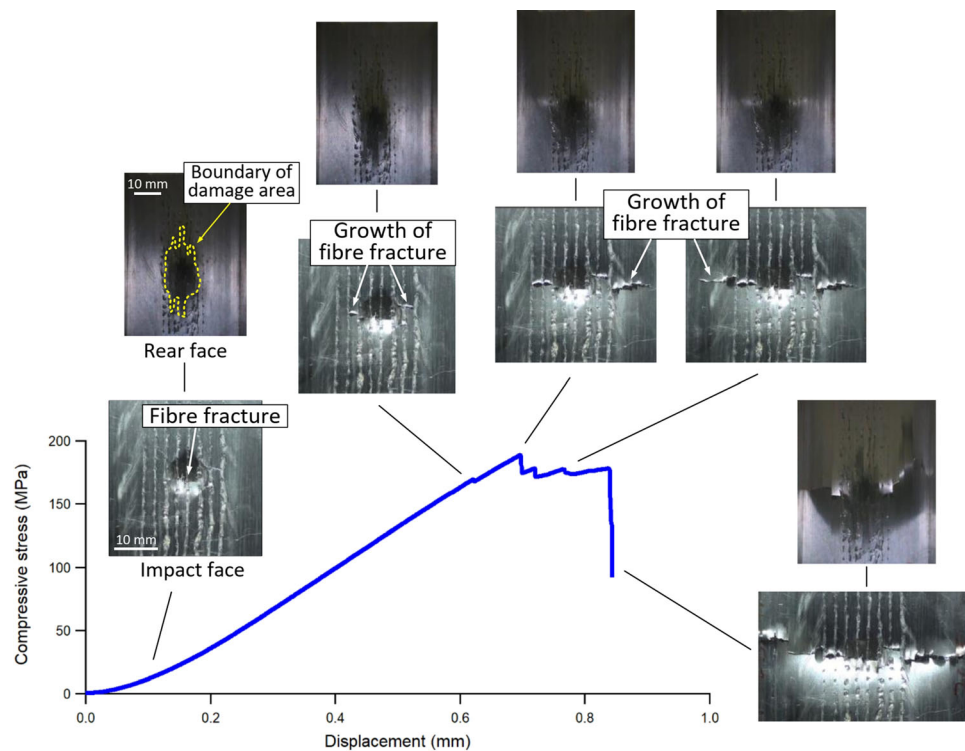


**Fig. 20** Progression of damage mechanisms observed during CAI loading on the front and rear faces of an unpinned sample impacted at 24 J

z-pins become effective at restraining delamination growth only for impact energies above this threshold value, i.e., when the impact delamination is large enough to activate the crack bridging tractions generated by z-pins. Reductions in delamination size of up to 50% are achieved by z-pinning for impacts with energies leading to perforation or penetration damage conditions.

(3) The CAI strength is degraded by z-pinning on samples impacted with energies approximately below the threshold of 6 J, while it is clearly improved on samples subjected to higher impact energies, with improvements of the order of 20% for perforation and penetration damage.

(4) The decrease in CAI strength observed after z-pinning for low impact energies is due to the adverse effect of
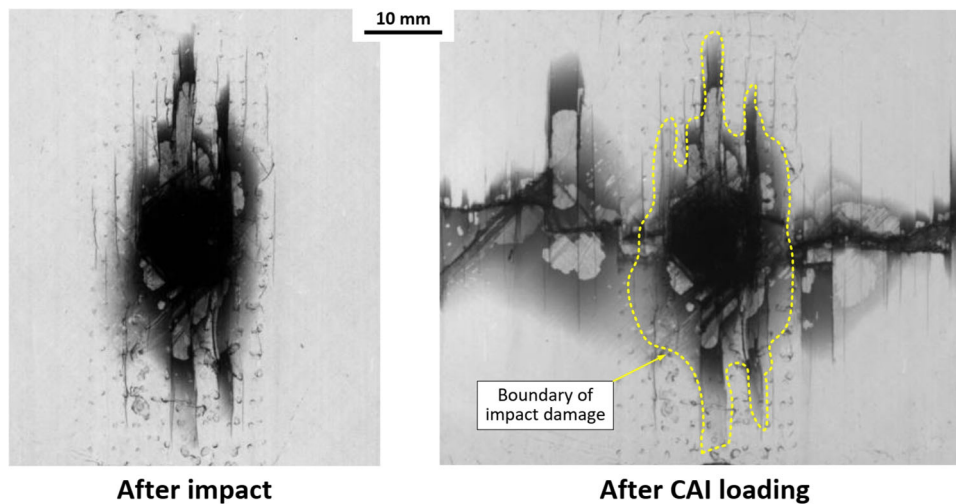
**Fig. 21** X-radiographs of an unpinned sample impacted at 24 J acquired before (left) and after CAI loading (right)



**Fig. 22** Progression of damage modes observed during CAI loading on the front and rear faces of a z-pinned sample impacted at 24 J

the fiber damage introduced during the z-pinning process. The improvements in the CAI performance achieved by z-pinning for higher impact energies may be attributed to the contribution of two concurring beneficial factors: the reduction of impact delamination size and the higher stiffness of the delaminated regions bridged by through-thickness z-pins.

(5) The final event triggering the CAI collapse of the laminate is the unstable propagation of broken fibers from the indentation area, while no growth of the pre-existing impact-induced delamination occurs during CAI loading. The extent and features of impact damage were observed to significantly affect the role of z-pins on the progression of the damage mechanisms leading to final CAI failure.

**Fig. 23** X-radiographs of a z-pinned sample impacted at 24 J taken before (left) and after CAI loading (right)
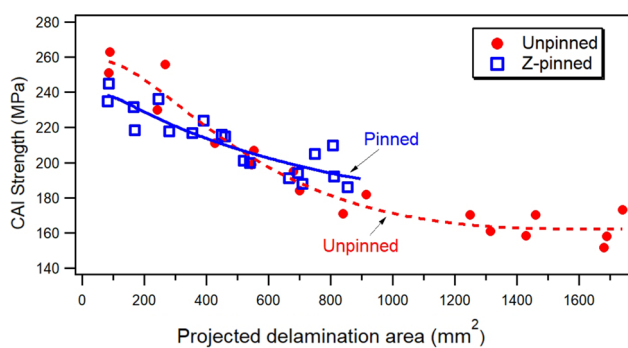


**Fig. 24** CAI strength versus delamination area for unpinned and z-pinned samples

## Funding

## Open Access

## References

1. V. Lopresto and G. Caprino, Damage Mechanisms and Energy Absorption in Composite Laminates Under Low Velocity Impact Loads, Dynamic Failure of Composite and Sandwich Structures, *Dordrecht*. S. Abrate, B. Castanié, Y.D.S. Rajapakse Ed., Springer, Netherlands, 2013

2. M.R. Wisnom, The Role of Delamination in Failure of Fibre-Reinforced Composites, *Phil. Trans. R. Soc. A*, 2012, **370**, p 1850–1870.

3. L. Tong, A.P. Mouritz and M.K. Bannister, *3D Fibre Reinforced Polymer Composites*, Elsevier, Oxford, 2002

4. I.K. Partridge, D.D.R. Cartié and T. Bonnington, Manufacture and Performance of Z-Pinned Composites, Advanced Polymeric Materials: Structure-Property Relationships, *Boca Raton*. S. Advani, G. Shonaike Ed., CRC Press, USA, 2003

5. I.K. Partridge, M. Yasaee, G. Allegri and J.K. Lander, Damage-Tolerant Composite Structures by Z-Pinning, Toughening Mechanisms in Composite Materials, *Sawston, Cambridge*. Q. Qin, J. Ye Ed., Elsevier, Netherlands, 2015

6. I.K. Partridge and D.D.R. Cartié, Delamination Resistant Laminates by Z-Fiber Pinning: Part I-Manufacture and Fracture Performance, *Compos. A Appl. Sci. Manuf.*, 2005, **36**(1), p 55–64.

7. A.P. Mouritz and B.N. Cox, A Mechanistic Interpretation of the Comparative In-Plane Mechanical Properties of 3D Woven, Stitched and Pinned Composites, *Compos. A Appl. Sci. Manuf.*, 2010, **41**(6), p 709–728.

8. K. Pingkarawat and A.P. Mouritz, Improving the Mode I Delamination Fatigue Resistance of Composites using Z-Pins, *Comp. Sci. Tech.*, 2014, **92**, p 70–76.

9. M. Knaupp, F. Baudach, J. Franck and G. Scharr, Mode I and Pull-Out Tests of Composite Laminates Reinforced with Rectangular Z-Pins, *J. Compos. Mater.*, 2014, **48**(23), p 2925–2932.

10. F. Pegorin, K. Pingkarawat, S. Daynes and A.P. Mouritz, Influence of Z-Pin Length on the Delamination Fracture Toughness and Fatigue Resistance of Pinned Composites, *Compos. B. Eng.*, 2015, **78**, p 298–307.

11. P. Chang, A.P. Mouritz and B.N. Cox, Properties and Failure Mechanisms of Pinned Composite Lap Joints in Monotonic and Cyclic Tension, *Compos. A Appl. Sci. Manuf.*, 2006, **66**(13), p 2163–2176.

12. A.P. Mouritz, Compression Properties of Z-Pinned Composite Laminates, *Compos. Sci. Technol.*, 2007, **67**, p 3110–3120.

13. R. Li, N. Huong, A. Crosky, A.P. Mouritz, D. Kelly and P. Chang, Improving Bearing Performance of Composite Bolted Joints Using Z-Pins, *Compos. Sci. Technol.*, 2009, **69**, p 883–889.

14. L. Francesconi and F. Aymerich, Effect of Z-Pinning on the Impact Resistance of Composite Laminates with Different Layups, *Compos. A Appl. Sci. Manuf.*, 2018, **114**, p 136–148.

15. N. Sarantinos, S. Tsantzalis, S. Ucsnik and V. Kostopoulos, Review of Through-The-Thickness Reinforced Composites in Joints, *Compos. Struct.*, 2019, **229**, p 111404.

16. A.P. Mouritz, Review of Z-Pinned Laminates and Sandwich Composites, *Compos. A Appl. Sci. Manuf.*, 2020, **139**, p 106128.

17. V. Kostopoulos, N. Sarantinos and S. Tsantzalis, Review of Through-the-Thickness Reinforced Z-Pinned Composites, *J. Compos. Sci.*, 2020, **4**(1), p 31.

18. L. Francesconi and F. Aymerich, Damage Mechanisms in the CAI Failure of Thin Z-Pinned Composite Laminates, *Compos. A Appl. Sci. Manuf.*, 2022, **158**, p 106991.

19. P. Chang, A.P. Mouritz and B.N. Cox, Flexural Properties of Z-Pinned Laminates, *Compos. A Appl. Sci. Manuf.*, 2007, **38**, p 244–251.

20. J. Hoffmann and G. Scharr, Compression Properties of Composite Laminates Reinforced with Rectangular Z-Pins, *Compos. Sci. Technol.*, 2018, **167**, p 463–469.

21. A. Knopp and G. Scharr, Tensile Properties of Z-Pin Reinforced Laminates with Circumferentially Notched Z-Pins, *J. Compos. Sci.*, 2020, **4**(2), p 78.

22. X. Zhang, L. Hounslow and M. Grassi, Improvement of Low-Velocity Impact and Compression-After-Impact Performance by Z-Fibre Pinning, *Compos. Sci. Technol.*, 2006, **66**(15), p 2785–2794.

23. M.D. Isa, S. Feih and A.P. Mouritz, Compression Fatigue Properties of Z-Pinned Quasi-Isotropic Carbon/Epoxy Laminate with Barely Visible Impact Damage, *Compos. Struct.*, 2011, **93**(9), p 2269–2276.

24. A.P. Mouritz, Delamination Properties of Z-Pinned Composites in Hot-Wet Environment, *Compos. A Appl. Sci. Manuf.*, 2013, **52**, p 134–142.

25. ASTM D7137/D7137M-12. Compressive residual strength properties of damaged polymer matrix composite plates, ASTM International, West Conshohocken, PA

26. K.T. Tan, N. Watanabe and Y. Iwahori, Impact Damage Resistance, Response, and Mechanisms of Laminated Composites Reinforced by Through-Thickness Stitching, *Int. J. Damage Mech.*, 2012, **21**, p 51–80.

27. L. Francesconi and F. Aymerich, Numerical Simulation of the Effect of Stitching on the Delamination Resistance of Laminated Composites Subjected to Low-Velocity Impact, *Compos. Struct.*, 2017, **159**, p 110–120.